

**CHEMICALLY REACTIVE MHD FLOW THROUGH A
SLENDERING STRETCHING SHEET SUBJECTED TO
NON-LINEAR RADIATION FLOW OVER A LINEAR AND
NON-LINEAR STRETCHING SHEET**

Mariam Sheikh¹, Jafar Hasnain², Nomana Abid² and Zaheer Abbas³

¹ Department of Mathematics, Faculty of Sciences
University of Sialkot, 51310 Sialkot, Pakistan

² Department of Computer Sciences
Bahria University Islamabad Campus, 44100 Islamabad, Pakistan

³ Department of Mathematics
The Islamia University of Bahawalpur 63100 Bahawalpur, Pakistan

Abstract. In this analysis, the MHD flow and n^{th} -order dispersion of chemically reactive species over a slendering stretching sheet are studied numerically. The partial slip boundary condition and non-linear form of thermal radiation are also considered in this research. To get non-linear ordinary differential equations from the system of partial differential equations governing the flow, energy, and concentration, similarity transformations are applied. Using the shooting technique and the Runge-Kutta scheme, the resultant equations are integrated numerically. The numerical results in terms of temperature, velocity, and concentration are represented graphically. Results from this research indicate that an increase in the wall thickness parameter reduces momentum and heat transfer effects when a magnetic field is present.

Keywords: Chemically reactive fluid, MHD slip flow, slendering stretching sheet, non-linear Rosseland thermal radiation.

Received April 13, 2023, revised: October 02, 2023, accepted: January 05, 2024

Communicated by Miloš Ivanović

Corresponding Author: Mariyam Sheikh. E-mail addresses: mariam_sheikh23@yahoo.com (M. Sheikh), jafar_hasnain14@yahoo.com (J. Hasnain), nomanaabid7890@gmail.com (N. Abid), za_qau@yahoo.com (Z. Abbas)

2020 *Mathematics Subject Classification.* Primary 76D05; Secondary 80A21, 80A32

© 2024 BY UNIVERSITY OF NIŠ, SERBIA | CREATIVE COMMONS LICENSE: CC BY-NC-ND

1. Introduction

The combined analysis of heat and momentum transport with a chemical reaction (CR) on a constantly moving sheet has a significant role in many processes due to which these problems obtained a lot of attention recently. These developments include surface evaporation of the water body, transfer of heat in a misty refrigerating tower, drying, and the stream within a desert cooler. After the innovative study of Sakiadis [29], who investigated BLF beyond a constant solid surface, many researchers studied this problem with various aspects. Crane [10] studied the flow past a stretching plate. In a numerical study, the characteristics of heat and mass transport with n th-order CR over a linearly SS were discussed by Ferdows and Al-Mdallal [14]. Makinde et al. [22] described the effects of BL flow with the transmission of convective temperature at the surface in the existence of thermal diffusion and MHD. Rashidi et al. [26] examined the heat and mass transport with free convection in magnetohydrodynamic liquid flow under the effects of buoyancy force and radiation past SS. Mabood et al. [20] studied the combined heat and mass transport impacts on magnetohydrodynamic fluid flow through SS under the impact of first-order CR. Babu and Sandeep [5, 4, 6] inspected the hydromagnetic flow past a slendering stretching sheet (SS) along with various presumptions. All the above studies discussed the fluid flow over a flat SS with different assumptions and physical geometries. In real-world applications, the SS not necessarily be flat, we may be confronted by sheets with variable thickness (VT). Plates having VT are commonly present in acoustical components, nuclear reactor technology, naval structures, and machine design and are also one of the essential characteristics in the investigation of orthotropic plate vibration. Initially, Lee [19] discussed the idea of needles by considering VT and solved the problem numerically. Later, Fang et al. [13] analyzed the boundary layer (BL) flow over SS with VT. Khader and Megahed [18] presented the numerical solution of Newtonian fluid flow through a non-linear SS with VT and velocity slip condition (SC). Subhashini et al. [31] investigated the two-fold solutions of two-dimensional laminar thermal diffusive flows past SS with VT. The ramifications of the magnetohydrodynamic nanofluid flow comprising Ag and TiO_2 nanoparticles through a slender SS with VT are analyzed by Acharya et al. [2]. Babu et al. [7] deliberated the dissipative hydromagnetic flow with the influence of temperature-dependent variable viscosity over a slender SS. The radiative effects on hydromagnetic fluid with heat and mass transport have several important practical applications i.e., in astrophysical power technology, planetary vehicle re-entry, electronic power manufacturing, removal of nuclear surplus and suspension of chemical impurities through water-saturated dust, and many more. Magyari and Pantokratoras [21] inspected the effect of thermal radiation (TR) on various BL flows using linearized Rosseland approximation. Mushtaq et al. [24] studied the impacts of nonlinear TR on the two-dimensional viscous flow of nanoliquids because of the presence of solar energy. Devi and Prakash [11] explored the influences of TR on hydromagnetic liquid flow past a slendering SS. Qayyum et al. [28] scrutinized the third-grade MHD nanofluid flow over a slendering SS under the effects of heat generation/absorption and TR heat. A radiative ferrofluid flow along with the impact of aligned magnetic field and frictional heating through a slendering

SS is examined by Reddy et al. [27]. Mousavi et al. [23] explored the dual solutions for water-based TiO_2 -Cu nanofluid flow in the presence of TR over a continuously moving thin needle. Due to the significance of slip flow in many industrial thermal problems and manufacturing fluid dynamics, slip effects with various configurations have been analyzed in the literature. Wang [33] discussed the flow through a SS in the existence of partial slip. In another study, Wang [32] explored the viscous flow over a SS under the impacts of velocity SC and suction force. Fang et al. [12] analytically explained the MHD viscous flow problem with slip condition over SS. BL flow with fixed heat flux surface and velocity SC through a uniform plate was deliberated by Aziz [3]. For a BL flow, Hayat et al. [16] deliberated the hydro-magnetic flow and heat transport characteristics over SS with velocity and thermal SCs. Bhattacharyya et al. [8] inspected the BL forced convective flow past a porous plate. Velocity and thermal SCs were also considered. Ibrahim and Shankar [17] examined the heat transport and BL flow of nano liquid past SS with solutal slip BCs. Hasnain et al. [15] deliberated the outcomes of velocity slip on dusty ferrofluid in a channel through spongy media. In the existing exploration, we analyze the impact of n th-order CR on the hydromagnetic viscous liquid past a continually moving sheet with VT. The non-linear TR and slip boundary conditions towards a sheet are also considered. A numerical technique is employed to get the approximate solution of obtained coupled non-linear PDEs. The influence of the Hartman number, the parameter of wall thickness, the radiation parameter, the Schmidt number, and the parameter of velocity power index on liquid velocity, temperature, and concentration profiles is examined through their graphic illustrations.

2. Problem development

The two-dimensional, laminar, and time-independent flow of Newtonian liquid under the effects of Lorentz force with constant density through an impermeable SS with BL and VT is considered. The sheet is situated in the xz -plane, the x -axis is towards the motion of SS however y -axis is considered vertically. The SS velocity is assumed as $U_w(x) = U_0(x+b)^m$. We further suppose that the thickness of the sheet is not fixed and is written as $y = A(x+b)^{(1-m)/2}$. To do away with the pressure gradient, a small enough value of A is chosen to make the sheet thin enough. The magnetic field $B(x) = B_0(x+b)^{(m-1)/2}$ is taken vertically upward to fluid flow. Because of the supposition of neglectable magnetic Reynolds number, the outer electric field is insignificant and there is no effect of an induced magnetic field. Figure 2.1 signifies the physical model of a slendering SS along with varying thickness. For this problem, we take $m \neq 1$, it is because the sheet becomes flat by considering $m = 1$. Moreover, non-linear TR is considered in the present numerical analysis. Under these physical considerations, the mathematical model for the proposed boundary layer flow is specified as

$$(2.1) \quad \frac{\partial u}{\partial x} + \frac{\partial v}{\partial y} = 0,$$

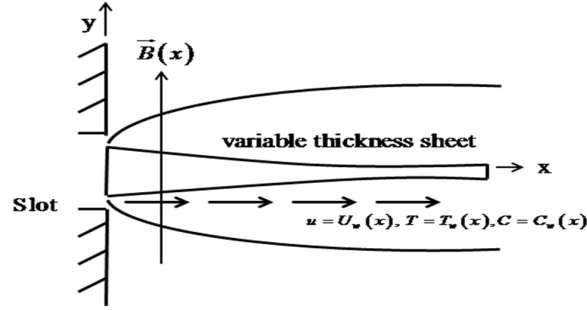


FIG. 2.1: Physical model of a slendering SS along with varying thickness

$$(2.2) \quad u \frac{\partial u}{\partial x} + v \frac{\partial u}{\partial y} = v \frac{\partial^2 u}{\partial y^2} - \frac{\sigma B(x)^2 u}{\rho},$$

$$(2.3) \quad u \frac{\partial T}{\partial x} + v \frac{\partial T}{\partial y} = \frac{k}{\rho c_p} \frac{\partial^2 T}{\partial y^2} - \frac{1}{\rho c_p} \frac{\partial q_r}{\partial y},$$

$$(2.4) \quad u \frac{\partial C}{\partial x} + v \frac{\partial C}{\partial y} = D \frac{\partial^2 C}{\partial y^2} - k_n(x) (C - C_\infty)^n,$$

where $k_n(x) = k(b+x)^{(m-1)(n+1)/2}$ represents the change of n^{th} -order homogeneous CR.

The relevant BCs of heat, momentum, and concentration fields are:

$$(2.5) \quad \begin{aligned} u(x, y) &= U_w(x) + h_1^* \left(\frac{\partial u}{\partial y} \right), \\ v(x, A(x+b)^{\frac{1-m}{2}}) &= 0, \\ T(x, y) &= T_w(x) + h_2^* \left(\frac{\partial T}{\partial y} \right), \\ C(x, y) &= C_w(x) + h_3^* \left(\frac{\partial C}{\partial y} \right), \quad \text{at } y = A(x+b)^{\frac{1-m}{2}}, \\ u(x, \infty) &= 0, T(x, \infty) = T_\infty, C(x, \infty) = C_\infty, \quad (m \neq 1) \end{aligned}$$

here

$$\begin{aligned} h_1^* &= \left[\frac{2-f_1}{f_1} \right] \xi_1 (x+b)^{\frac{1-m}{2}}, \quad h_2^* = \left[\frac{2-a}{a} \right] \xi_2 (x+b)^{\frac{1-m}{2}}, \quad \xi_2 = \left(\frac{2\gamma_1}{\gamma_1+1} \right) \frac{\xi_1}{\text{Pr}}, \\ h_3^* &= \left[\frac{2-c}{c} \right] \xi_3 (x+b)^{\frac{1-m}{2}}, \quad \xi_3 = \left(\frac{2\gamma_2}{\gamma_2+1} \right) \frac{\xi_1}{Sc}. \end{aligned}$$

To obtain a similar solution we considered a special form of wall temperature and wall concentration defined as (Subhashini et al. [31])

$$(2.6) \quad T_w(x) = T_0(x+b)^{\frac{1-m}{2}} + T_\infty, \quad C_w(x) = C_0(x+b)^{\frac{1-m}{2}} + C_\infty, \quad (m \neq 1).$$

Applying Rosseland approximation for optically thick medium, the radiation heat flux is taken as (Raptis [25], Brewster [9], and Sparrow and Cess [30])

$$(2.7) \quad q_r = -\frac{4\sigma^*}{k^*} \frac{\partial T^4}{\partial y} = -\frac{16\sigma^*}{3k^*} T^3 \frac{\partial T}{\partial y}.$$

By using Eq. (2.7) in Eq. (2.3), we get

$$(2.8) \quad u \frac{\partial T}{\partial x} + v \frac{\partial T}{\partial y} = \frac{\partial}{\partial y} \left[\left(\alpha + \frac{16\sigma^* T^3}{3k^* \rho c_p} \right) \frac{\partial T}{\partial y} \right].$$

Similarity transformations in the following form are considered to simplify the flow problem (see Khader and Megahed [18])

$$(2.9) \quad \eta = y \sqrt{\frac{m+1}{2} \frac{U_0 (x+b)^{m-1}}{v}}, \quad u = U_0 (x+b)^m f'(\eta),$$

$$v = -\sqrt{\frac{m+1}{2} v U_0 (x+b)^{m-1}} \left[f'(\eta) \eta \left(\frac{m-1}{m+1} \right) + f(\eta) \right], \quad (m \neq 1),$$

$$\theta = \frac{T - T_\infty}{T_w(x) - T_\infty} \quad \text{with} \quad T = T_\infty (1 + (\theta_w - 1)\theta),$$

$$\theta_w = \frac{T_w}{T_\infty}, \quad \phi = \frac{C - C_\infty}{C_w(x) - C_\infty},$$

Using similarity transformations (2.9), the continuity Eq. (2.1) is inevitably fulfilled and Eqs. (2.2), (2.4) and (2.8) with BCs (2.5) take the form

$$(2.10) \quad f''' = \left(\frac{2m}{m+1} \right) (f')^2 - f f'' + M^2 f',$$

$$(2.11) \quad \left(1 + R_d (1 + (\theta_w - 1)\theta)^3 \theta' \right)' = \text{Pr} \left(\left(\frac{1-m}{m+1} \right) f' \theta - f \theta' \right),$$

$$(2.12) \quad \phi'' = Sc \left(\left(\frac{1-m}{m+1} \right) f' \phi - f \phi' \right) + Sc \gamma \phi^n.$$

with

$$(2.13) \quad f(\lambda) = \lambda \left(\frac{1-m}{m+1} \right) (1 + h_1 f''(\lambda)), \quad f'(\lambda) = 1 + h_1 f''(\lambda),$$

$$\theta(\lambda) = 1 + h_2 \theta'(\lambda), \quad \phi(\lambda) = 1 + h_3 \phi'(\lambda),$$

$$f'(\infty) = 0, \quad \theta(\infty) = 0, \quad \phi(\infty) = 0, \quad (m \neq 1),$$

where

$$R_d = \frac{16\sigma^* T_\infty^3}{3kk^*}, \quad M^2 = \frac{2\sigma B_0^2}{(1+m)\rho U_0}, \quad \gamma = \frac{2k C_0^{n-1}}{(1+m)U_0}, \quad \text{Pr} = \frac{v}{\alpha}, \quad Sc = \frac{v}{D}.$$

Moreover, $R_d = 0$ shows no TR effect, > 0 represents the destructive CR whereas < 0 represents the constructive CR and

$$\lambda = A\sqrt{\frac{U_0(m+1)}{2\nu}}, \quad h_1 = \left[\frac{2-f_1}{f_1} \right] \xi_1 \sqrt{\frac{U_0(m+1)}{2\nu}},$$

$$h_2 = \left[\frac{2-a}{a} \right] \xi_2 \sqrt{\frac{U_0(m+1)}{2\nu}}, \quad h_3 = \left[\frac{2-c}{c} \right] \xi_3 \sqrt{\frac{U_0(m+1)}{2\nu}}.$$

The domain of Eqs. (2.10)-(2.12) with BC's Eq. (2.13) is $[\lambda, \infty]$. To accommodate the calculation we transform domain $[\lambda, \infty]$ into $[0, \infty]$, for this let $F(\xi)=F(\eta-\lambda)=f(\eta)$. Using this transformation Eqs. (2.10)-(2.12) become

$$(2.14) \quad F''' = \left(\frac{2m}{m+1} \right) (F')^2 - FF'' + M^2 F',$$

$$(2.15) \quad \left(1 + R_d(1 + (\theta_w - 1)\Theta)^3 \Theta' \right)' = \text{Pr} \left(\left(\frac{1-m}{m+1} \right) F'\Theta - F\Theta' \right),$$

$$(2.16) \quad \Phi'' = Sc \left(\left(\frac{1-m}{m+1} \right) F'\Phi - F\Phi' \right) + Sc\gamma \Phi^n,$$

and the BC's are

$$(2.17) \quad \begin{aligned} F(0) &= \lambda \left(\frac{1-m}{m+1} \right) (1 + h_1 F''(0)), & F'(0) &= 1 + h_1 F''(0), \\ \Theta(0) &= 1 + h_2 \Theta'(0), & \Phi(0) &= 1 + h_3 \Phi'(0), \\ F'(\infty) &= 0, & \Theta(\infty) &= 0, & \Phi(\infty) &= 0, & (m \neq 1). \end{aligned}$$

The skin-drag parameter C_f , the local Nusselt number Nu_x and the local Sherwood number Sh_x are defined as

$$(2.18) \quad C_f = \frac{1}{\frac{1}{2}\rho U_w^2 \mu} \left. \frac{\partial u}{\partial y} \right|_{y=A(x+b)^{\frac{1-m}{2}}} = 2\sqrt{\frac{m+1}{2}} (Re_x)^{-\frac{1}{2}} F''(0),$$

$$(2.19) \quad \begin{aligned} Nu_x &= -\frac{(x+b)}{(T_w(x) - T_\infty)} \left. \frac{\partial T}{\partial y} \right|_{y=A(x+b)^{\frac{1-m}{2}}} + (q_r)_w = \\ &= -\sqrt{\frac{m+1}{2}} (1 + R_d\theta_w^3) (Re_x)^{\frac{1}{2}} \Theta'(0), \end{aligned}$$

$$(2.20) \quad Sh_x = -\frac{(x+b)}{(C_w(x) - C_\infty)} \left. \frac{\partial C}{\partial y} \right|_{y=A(x+b)^{\frac{1-m}{2}}} = -\sqrt{\frac{m+1}{2}} (Re_x)^{\frac{1}{2}} \Phi'(0),$$

where $Re_x = U_w X/\nu$ and $X=(x+b)$ is the local Reynolds number.

3. Numerical scheme

Non-linear differential equations (2.14)-(2.16) with boundary conditions (2.17) are solved using the shooting technique together with the fourth-order Runge-Kutta method. Our system of equations must be transformed into a first-order initial value system for this technique by declaring:

$$(3.1) \quad y_1 = F, y_2 = F', y_3 = F'', y_3' = \left(\frac{2m}{m+1} \right) y_2^2 - y_1 y_3 + M^2 y_2,$$

$$y_4 = \Theta, y_5 = \Theta',$$

$$(3.2) \quad y_5' = \frac{1}{1 + R_d(1 + (\theta_w - 1)y_4)^3} \left(-3R_d(1 + (\theta_w - 1)y_4)^2(\theta_w - 1)y_5^2 \right)$$

$$- \frac{1}{1 + R_d(1 + (\theta_w - 1)y_4)^3} \left((1 + R_d(\theta_w - 1)y_4)^3 \right) y_5$$

$$+ \frac{1}{1 + R_d(1 + (\theta_w - 1)y_4)^3} \left(Pr \left(\left(\frac{1-m}{m+1} \right) y_2 y_4 - y_1 y_5 \right) \right),$$

$$(3.3) \quad y_6 = \Phi, y_7 = \Phi', y_7' = Sc \left(\left(\frac{1-m}{m+1} \right) y_2 y_6 - y_1 y_7 \right) + Sc\gamma (y_6)^n,$$

with boundary conditions

$$y_1(0) = \lambda \left(\frac{1-m}{m+1} \right) (1 + h_1 u_1), \quad y_2(0) = 1 + h_1 u_1, \quad F''(0) = u_1,$$

$$y_4(0) = 1 + h_2 u_2, \quad \Theta' = u_2, \quad y_7(0) = 1 + h_3 u_3, \quad \Phi' = u_3.$$

4. Results and discussion

The solution of ODE's (2.14)-(2.16) with BC's (2.17) is numerically determined by using the shooting method together with the 4th-order algorithm of Runge-Kutta. The influences of all involved constraints on the momentum, concentration, and temperature inside the BL are displayed in Figures 4.1-4.6.

The effect of Hartman number M on liquid velocity is seen in Figure 4.1a. Slip and no-slip velocity conditions are taken into consideration. It is evident from Figure 4.1a that both the liquid velocity and BL thickness decline with an increase in M for both slip and no-slip conditions. Lorentz force (a force manifesting owing to the combined action of magnetic and electric fields) is responsible for this attenuation since it works against transport phenomena more potently. Figure 4.1b represents the variation of wall thickness parameter λ and power index parameter m on liquid velocity. It is observed from this Figure that augmentation in m causes an upsurge in sheet slenderness which enables the fluid to flow more rapidly due to this flow velocity accelerates and ultimately boundary layer thickness becomes

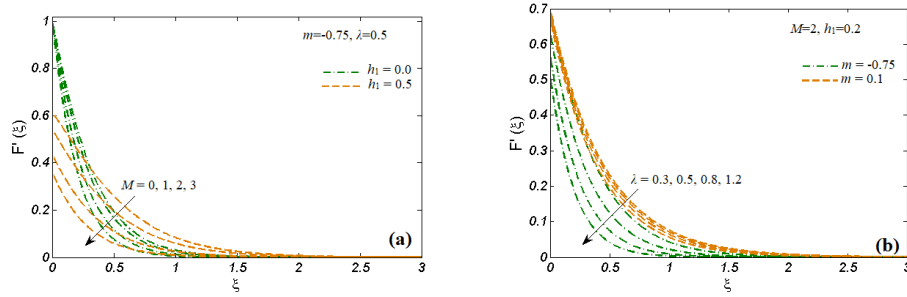


FIG. 4.1: Momentum transfer for distinct values of (a) M and h_1 (b) λ and m .

thicker. However, the parameter of the wall thickness λ creates retardation in the flow velocity and consequently, BL thickness reduces with a rise in wall thickness parameter λ .

Figure 4.1a exhibits the influences of the M on dimensionless temperature. It is detected that the temperature profiles enhance when Hartman number M is increased, and results are the same when we consider velocity slip as well as non-slip velocity. Since Lorentz force acts as a resistive force for fluid movement thus heat is generated and therefore the thermal BL thickness rises when M escalates. Figure 4.1b displays the variation of the power index of velocity m and thickness of wall parameter λ on the temperature of the liquid. It is depicted that both the thickness of thermal BL and temperature is the increasing function of m whereas decreases with increasing wall thickness parameter λ . Heat transfers faster through the thinner surface and in this case, an increase in m tends to reduce sheet thickness. As a result, a higher value for m leads to a hotter temperature profile.

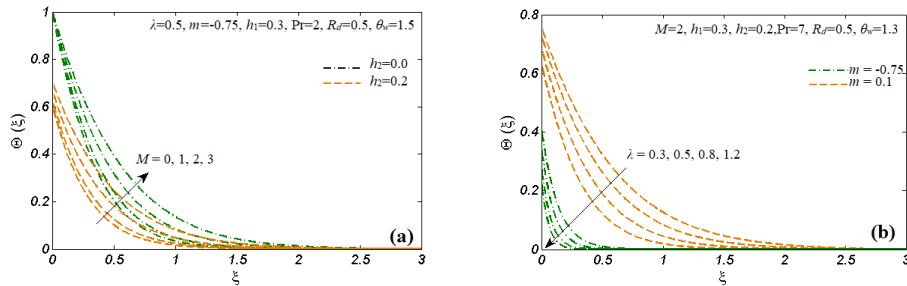


FIG. 4.2: Heat transfer for distinct values of (a) M and h_2 (b) m and λ

Figure 4.3a is illustrated to show the variation in the temperature profiles for Pr and Rd . It is noticed from this fig. that the temperature profiles along with thermal BL thickness decrease with high Pr . Physically, the thermal diffusivity falls when Pr increases therefore heat is diffused slowly far from the heated sheet. However, the temperature profiles and thickness of thermal BL augments with increments in

radiation parameter R_d . Figure 4.3b is the graphical depiction of variation in θ_w for temperature profiles. It is detected that heat travels effectively as thickness for thermal BL is found to grow with θ_w .

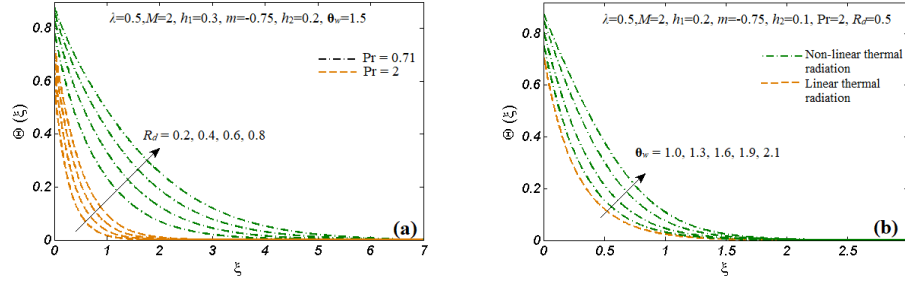


FIG. 4.3: Heat transport for distinct values of (a) R_d and Pr (b) θ_w

The influence of M on the concentration profile is demonstrated in Figure 4.4a. Both the concentration and thickness of its BL are found to increase with M , and this is true for both the slip and no-slip scenarios. The fluid experiences friction due to Lorentz force by accumulative friction among the layers, which is why species distribution increases. Figure 4.4b reveals the behavior of species concentration for different values of m and λ . It shows that species concentration enhances when m is increased and falls with the augmentation in λ . As the temperature of the liquid escalates with m , the species concentration also increases. Comparison of the

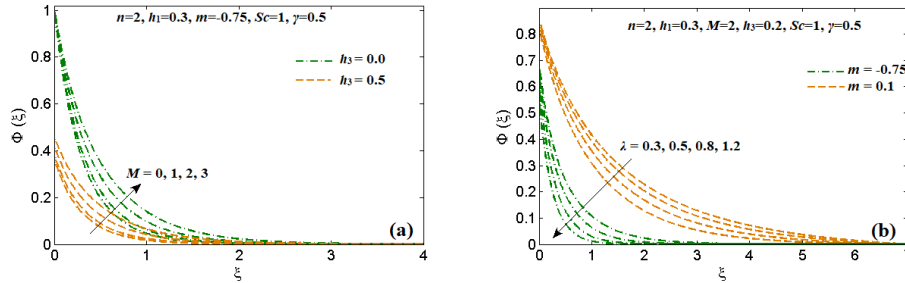


FIG. 4.4: Concentration profile for distinct values of (a) M and h (b) λ and m .

effects of no-slip velocity vs slip velocity on species concentration as a function of Sc are shown in Figure 4.5a. Schmidt number describes the ratio of the viscous BL thickness and thickness of the concentration BL so from this figure, we see that increasing Schmidt number Sc decreases the solute BL. Figure 4.5b displays the impacts of the rate of CR parameter on the species concentration for no-slip velocity and slip velocity conditions. For both cases, the liquid concentration decreases for destructive CR ($\gamma > 0$) and increases for constructive CR ($\gamma < 0$). Destructive CR behaves similarly to Schmidt number therefore, with destructive CR thickness of

solute BL falls while it increases with constructive CR. Therefore, the reaction rate is important in adjusting the solute BL in the reactive concentration distribution.

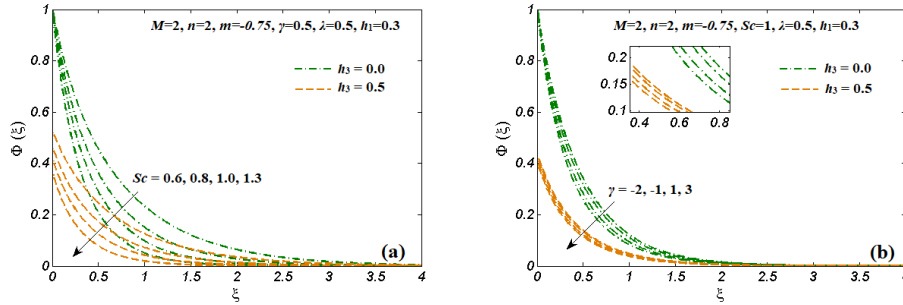


FIG. 4.5: Concentration behavior for distinct values of (a) Sc and h_3 (b) γ and h_3 .

Figure 4.6a shows the influence of both parameters λ and velocity power index m on $F''(0)$. Figure 4.6b illustrates the upshot of $\Theta'(0)$ with λ for distinct values of R_d . $\Theta'(0)$ increases with λ , while diminishes with increasing values of R_d . Figure 4.6c depicts that $\Phi'(0)$ is increased with an increment in Sc and λ . It is also depicted from this figure that $\Phi'(0)$ falls with the higher values of reaction-order parameter n .

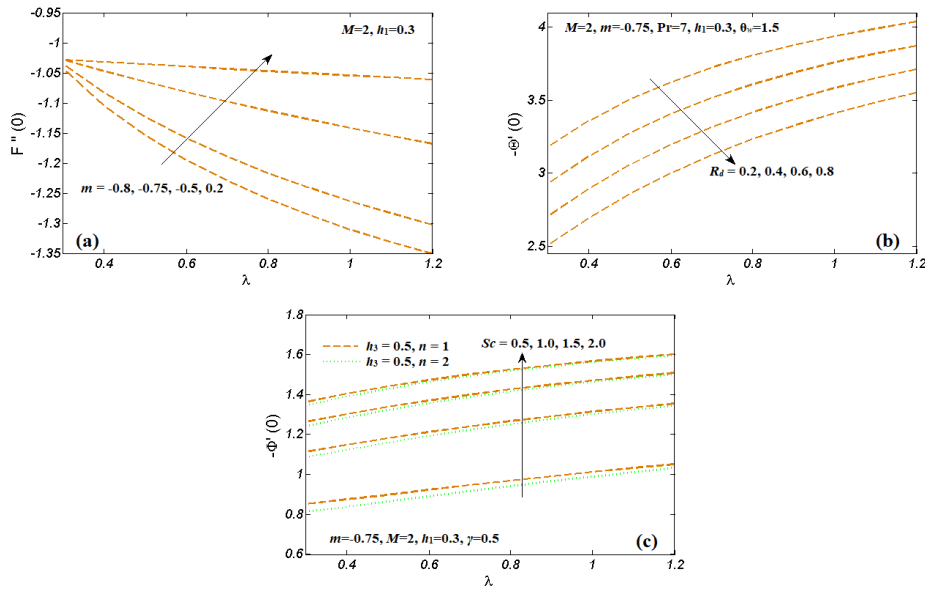


FIG. 4.6: Upshot of (a) $F''(0)$ for m (b) $\Theta'(0)$ for R_d (c) $\Phi'(0)$ for Sc versus λ .

To ensure the accuracy of new results, we compared them to previous studies'

Table 4.1: Numerical comparative values of $F''(0)$ when $\lambda=0.5$ and $M=0$

m	Fang et al. [13] (Numerical Method)	Subhashini et al. [31] (Numerical Method)	Present Results (Numerical Method)
-0.51	-1.1859	-1.1860	-1.1860
-0.55	-1.2807	-1.2821	-1.2808
-0.60	-1.4522	-1.4531	-1.4522
-0.65	-1.7095	-1.7103	-1.7095
-0.70	-2.0967	-2.0974	-2.0967
-0.75	-2.6882	-2.6891	-2.6882
-0.80	-3.6278	-3.6282	-3.6278
-0.85	-5.2477	-5.2481	-5.2477
-0.90	-8.5457	-8.5463	-8.5457
-0.95	-18.5194	-18.5209	-18.5194
-0.99	-98.5034	-98.5046	-98.4642

Table 4.2: Comparison with the numerical and analytical solution for $F''(0)$ when $M=0$

m	λ	Fang et al. [13] (Shooting Method)	Abdel-wahed et al. [1] (Optimal homotopy asymptotic method)	Present Results
0.50	0.25	-0.93380	-0.92641	-0.93376
1.00		-1.00000	-1.00000	-1.00000
5.00		-1.11860	-1.12623	-1.11858
0.50	0.5	-0.97990	-0.96335	-0.97994
1.00		-1.00000	-1.00000	-1.00000
2.00		-1.02340	-1.03339	-1.02339

findings and discovered they were in good accord which is represented in Table 4.1. Table 4.2 compares the current results to both numerical and analytical approaches and shows that they are in good agreement.

5. CONCLUDING REMARKS

The present work of hydromagnetic flow and dispersion of CRS towards a slendering SS with slip condition has been studied. Non-linear Rosseland thermal radiation is also considered within heat transfer. A comparison with available literature is also carried out. The key effects of the existing study can be prescribed as below:

- Since the magnetic field creates a drag force, liquid velocity and thickness of BL reduce when Hartman number M for both slip and no-slip conditions is increased. Whereas, increasing values of the Hartman number M boosts the

heat transfer and concentration field.

- The velocity, temperature, and CRS concentration profiles fall with increment in the thickness of wall parameter λ however, rise with a velocity power index m .
- Both radiation parameter R_d and θ_w increase the temperature profiles.
- Prandtl and Schmidt's numbers decline the heat transfer and concentration field, respectively.
- Destructive CR ($\gamma > 0$) reduces while constructive CR $\gamma < 0$ enhances the species concentration with both slip and no-slip conditions.

Acknowledgments

We would like to thank the anonymous reviewers for their useful comments to improve the paper.

REFERENCES

1. M. S. ABDEL-WAHED, E. M. A. ELBASHBESHY and T. G. EMAM: *Flow and heat transfer over a moving surface with non-linear velocity and variable thickness in a nanofluid in the presence of Brownian motion*. Appl. Math. Comput. **254**, (2015), 49-62.
2. N. ACHARYA, K. DAS and P. K. KUNDU: *Ramification of variable thickness on MHD TiO₂ and Ag nanofluid flow over a slendering stretching sheet using NDM*. The European Physical J. Plus. **131** (2016), 1-16.
3. A. AZIZ: *Hydrodynamic and thermal slip flow boundary layer over a flat plate with constant heat flux boundary condition*. Commun. Non-linear Sci. Numer. Simul. **15**, (2010), 573580.
4. M. J. BABU and N. SANDEEP: *MHD non-Newtonian fluid flow over a slendering stretching sheet in the presence of cross-diffusion effects*. ALEX. ENG. J. **55** (2016), 2193-2201.
5. M. J. BABU and N. SANDEEP: *Three-dimensional MHD slip flow of nanofluids over a slendering stretching sheet with thermophoresis and Brownian motion effects*. ADV. POWDER TECHNOL. **27** (2016), 2039-2050.
6. M. J. BABU and N. SANDEEP: *3D MHD slip flow of a nanofluid over a slendering stretching sheet with thermophoresis and Brownian motion effects*. J. Mol. Liq. **222** (2016), 1003-1009.
7. M. J. BABU, N. SANDEEP, M. E. ALI and A. O. NUHAIT: *Magnetohydrodynamic dissipative flow across the slendering stretching sheet with temperature dependent variable viscosity*. Results Phys. **7** (2017), 1801-1807.
8. K. BHATTACHARYYA, S. MUKHOPADHYAY and G.C. LAYEK: *Steady boundary layer slip flow and heat transfer over a flat porous plate embedded in a porous media*. Petroleum Sci. Engn. **78**, (2011), 304309.

9. M. Q. BREWSTER: *Thermal radiative transfer properties*. New York: John Wiley and Sons, 1996.
10. L. J. CRANE: *Flow past a stretching plate*. *Z. Angew. Math. Phys.* **21** (1970), 645–647.
11. S. P. A. DEVI and M. PRAKASH: *Thermal radiation effects on hydromagnetic flow over a slendering stretching sheet*. *Brazil. Soc. Mech. Sci. Engng.* **38**, (2015), 423–431.
12. T. FANG, J. ZHANG and S. YAO: *Slip MHD viscous flow over a stretching sheet an exact solution*. *Commun. Non-linear Sci. Numer. Simul.* **14**, (2009), 37313737.
13. T. FANG, J. ZHANG and Y. ZHONG: *Boundary layer flow over a stretching sheet with variable thickness*. *Appl. Math. Comput.* **218** (2012), 7241–7252.
14. M. FERDOWS and M. A. QASEM: *Effects of order of chemical reaction on a boundary layer flow with heat and mass transfer over a linearly stretching sheet*. *Am. J. Fluid Dyn.* **2** (2012), 89–94.
15. J. HASNAIN, H.G. SATTI, M. SHEIKH and Z. ABBAS: *Study of double slip boundary condition on the oscillatory flow of dusty ferrofluid confined in a permeable channel*. *Facta Universitatis, Series.* **21**, (2023), 671–684.
16. T. HAYAT, M. QASIM and S. MESOUB: *MHD flow and heat transfer over a permeable stretching sheet with slip conditions*. *Int. J. Numer. Methods Fluids.* **66**, (2011), 963–975.
17. W. IBRAHIM and B. SHANKAR: *MHD boundary layer flow and heat transfer of a nanofluid past a permeable stretching sheet with velocity, thermal and solutal slip boundary conditions*. *Computers and Fluids.* **78**, (2013), 110.
18. MM. KHADER and A. M. MEGAHEDE: *Numerical solution for boundary layer flow due to a nonlinearly stretching sheet with variable thickness and slip velocity*. *Eur. Phys. J. Plus.* **128** (2013), 1–7.
19. L. L. LEE: *Boundary layer over a thin needle*. *Phys. Fluids.* **10** (1967), 820–822.
20. F. MABOOD, WA. KHAN and AI. MD. ISMAIL: *MHD stagnation point flow and heat transfer impinging on stretching sheet with chemical reaction and transpiration*. *Chem. Eng. J.* **273** (2015), 430–437.
21. E. MAGYARI and A. PANTOKRATORAS: *Note on the effect of thermal radiation in the linearized Rosseland approximation on the heat transfer characteristics of various boundary layer flows*. *Int. Commun. Heat Mass Tran.* **38**, (2011), 554556.
22. OD. MAKINDE, K. ZIMBA and O. A. BÉG: *Numerical study of chemically-reacting hydromagnetic boundary layer flow with Soret/Dufour effects and a convective surface boundary condition*. *IJTEE.* **4** (2012), 89–98.
23. S. M. MOUSAVI, M. N. ROSTAMI, M. YOUSEFI and S. DINARVAND: *Dual solutions for MHD flow of a water-based TiO₂-Cu hybrid nanofluid over a continuously moving thin needle in presence of thermal radiation*. *Rep. Mech. Eng.* **2**, (2021), 31–40.
24. A. MUSHTAQ, M. MUSTAFA, T. HAYAT and A. ALSAEDI: *Nonlinear radiative heat transfer in the flow of nanofluid due to solar energy: A numerical study*. *Int. Commun. J. Taiwan Inst. Chem. Engn.* **45**, (2014), 11761183.
25. A. RAPTIS: *Radiation and free convection flow through a porous medium*. *Int. Commun. Heat Mass Trans.* **25**, (1998), 28995.

26. M. M. RASHIDI, B. ROSTAMI, N. FREIDONIMEHR and S. ABBASBANDY: *Free convective heat and mass transfer for MHD fluid flow over a permeable vertical stretching sheet in the presence of the radiation and buoyancy effects*. Ain Shams Eng. J. **5** (2014), 901–912.
27. J. V. R. REDDY, V. SUGUNAMMA and N. SANDEEP: *Effect of frictional heating on radiative ferrofluid flow over a slendering stretching sheet with aligned magnetic field*. The Europ. Phys. J. Plus. **132**, (2017), 1-13.
28. Q. SAJID, T. HAYAT and A. ALSAEDI: *Thermal radiation and heat generation/absorption aspects in third grade magneto-nanofluid over a slendering stretching sheet with Newtonian conditions*. Physica B: Condensed Matter. **537**, (2018), 139-149.
29. B. C. SAKIADIS: *Boundary-layer behavior on continuous solid surfaces: I. Boundary-layer equations for two-dimensional and axisymmetric flow*. AICHE J. **7** (1961), 26–28.
30. E. M. SPARROW and R. D CESS: *Radiation heat transfer*. Washington: Hemisphere, 1978.
31. SV. SUBHASHINI, R. SUMATHI and I. POP: *Dual solutions in a thermal diffusive flow over a stretching sheet with variable thickness*. ICHMT. **48** (2013), 61–66.
32. C. Y. WANG: *Analysis of viscous flow due to a stretching sheet with surface slip and suction*. Nonlinear Anal: Real World Appl. **10**, (2009), 37580.
33. C. Y. WANG: *Flow due to a stretching boundary with partial slip: an exact solution of Navier Stokes equations*. Chem. Eng. Sci. Acta Mech. **57**, (2002), 37453747.